Multi-time-scale Optimal Scheduling of Integrated Energy System with Electric-thermal-hydrogen Hybrid Energy Storage Under Wind and Solar Uncertainties

Zhe Chen, Zhihao Li, Da Lin, Changjun Xie, *Member*, *IEEE*, and Zhewei Wang

***Abstract*—Hybrid energy storage is considered as an effective means to improve the economic and environmental performance of integrated energy systems (IESs). Although the optimal scheduling of IES has been widely studied, few studies have taken into account the property that the uncertainty of the forecasting error decreases with the shortening of the forecasting time scale. Combined with hybrid energy storage, the comprehensive use of various uncertainty optimization methods under different time scales will be promising. This paper proposes a multi-time-scale optimal scheduling method for an IES with hybrid energy storage under wind and solar uncertainties. Firstly, the proposed system framework of an IES including electric-thermal-hydrogen hybrid energy storage is established. Then, an hour-level robust optimization based on budget uncertainty set is performed for the day-ahead stage. On this basis, a scenario-based stochastic optimization is carried out for intra-day and real-time stages with time intervals of 15 min and 5 min, respectively. The results show that ① the proposed method improves the economic benefits, and the intra-day and real-time scheduling costs are reduced, respectively; ② by adjusting the uncertainty budget in the model, a flexible balance between economic efficiency and robustness in day-ahead scheduling can be achieved; ③ reasonable design of the capacity of electric-thermal-hydrogen hybrid energy storage can significantly reduce the electricity curtailment rate and carbon emissions, thus reducing the cost of system scheduling.**

***Index Terms*—Integrated energy system (IES), hybrid energy storage, multi-time-scale optimal scheduling, robust optimization, stochastic optimization, uncertainty, wind power, solar power.**

Manuscript received: June 28, 2024; revised: September 30, 2024; accepted: November 20, 2024. Date of CrossCheck: November 20, 2024. Date of online publication: December 13, 2024.

This work was supported by the Science and Technology Project of State Grid Zhejiang Electric Power Co., Ltd. "Research on coordinated optimal configuration and operation control technology for long-term and short-term hybrid energy storage considering multi-time scale matching requirements" (No. 5211DS230001).

Z. Chen, Z. Li (corresponding author), and D. Lin are with State Grid Zhejiang Electric Power Research Institute, Hangzhou 310000, China (e-mail: zchen331@163.com; lzh_ee@163.com; ld2009ee@163.com).

C. Xie and Z. Wang are with the School of Automation, Wuhan University of Technology, Wuhan 430070, China (e-mail: jackxie@whut. edu. cn; 247694@whut.edu.cn).

DOI: 10.35833/MPCE.2024.000606

NOMENCLATURE

A. Constants

η_p^{GT}, η_q^{GT}	Power generation and heat production efficiencies of gas turbine (GT)
η_q^{GB}, η_h^{EL}	Energy conversion efficiencies of gas boiler (GB) and electrolyzer (EL)
$\eta_p^{HFC}, \eta_c^{EC}, \eta_c^{AC}$	Energy conversion efficiencies of hydrogen fuel cell (HFC), electric chiller (EC), and absorption chiller (AC)
$\eta_C^{EES}, \eta_D^{EES}$	Charging and discharging efficiencies of electric energy storage (EES)
$\eta_C^{TES}, \eta_D^{TES}$	Charging and discharging efficiencies of thermal energy storage (TES)
$\eta_C^{HES}, \eta_D^{HES}$	Charging and discharging efficiencies of hydrogen energy storage (HES)
$\delta_{re}, \delta_q, \delta_g$	Carbon emission coefficients for renewable energy, natural gas netowrk, and grid
Γ_{WT}, Γ_{PV}	Uncertain budgets of wind and solar power forecasting errors
μ^{WT}, σ^{WT}	Mean and standard deviation of wind power forecasting errors
μ^{PV}, σ^{PV}	Mean and standard deviation of solar power forecasting errors
c_{CO2}	Carbon tax price
$C_{\min}^{EC}, C_{\max}^{EC}$	The minimum and maximum power limits of EC
$C_{\min}^{AC}, C_{\max}^{AC}$	The minimum and maximum power limits of AC
$\hat{e}_t^{WT}, \hat{e}_t^{PV}$	Empirical values of wind and solar power forecasting errors at time t
$\bar{e}^{WT}, \underline{e}^{WT}$	Upper and lower limits of wind power forecasting errors
$\bar{e}^{PV}, \underline{e}^{PV}$	Upper and lower limits of solar power forecasting errors
$H_{\min}^{HFC}, H_{\max}^{HFC}$	The minimum and maximum power limits of HFC
$H_{C,\max}^{HES}, H_{D,\max}^{HES}$	The maximum charging and discharging power of HES

$H_{C,\min}^{HES}, H_{D,\min}^{HES}$	The minimum charging and discharging power of HES
$\hat{P}_t^{WT}, \hat{P}_t^{PV}$	Forecasting values of wind and solar power at time t
$P_{down}^{GT}, P_{up}^{GT}$	Down and up ramp rate limits of GT
$P_{\min}^{GT}, P_{\max}^{GT}$	The minimum and maximum power limits of GT
$P_{C,\max}^{EES}, P_{D,\max}^{EES}$	The maximum charging and discharging power of EES
$P_{C,\min}^{EES}, P_{D,\min}^{EES}$	The minimum charging and discharging power of EES
$P_{\max}^{buy}, G_{\max}^{buy}$	The maximum electric and gas input power from grid and natural gas network
p_t^{grid}, p^{gas}	Electricity price at time t and natural gas price
$p_{cut}^{WT}, p_{cut}^{PV}$	Penalty costs of abandoning wind and solar power
p_{om}^{r}	Operation and maintenance cost of equipment r, $r \in \{GT, GB, EL, HFC, EC, AC, EES, TES, HES\}$
$P_{\min}^{EL}, P_{\max}^{EL}$	The minimum and maximum power limits of EL
$P_t^{load}, Q_t^{load}, H_t^{load}, C_t^{load}$	Electric, thermal, hydrogen, and cooling load power at time t
$Q_{\min}^{GB}, Q_{\max}^{GB}$	The minimum and maximum power limits of GB
$Q_{C,\max}^{TES}, Q_{D,\max}^{TES}$	The maximum charging and discharging power of TES
$Q_{C,\min}^{TES}, Q_{D,\min}^{TES}$	The minimum charging and discharging power of TES
$SOC_0^{EES}, SOC_0^{TES}, SOC_0^{HES}$	Initial states of charge (stored energies) of EES, TES, and HES
$SOC_{\max}^{EES}, SOC_{\min}^{EES}$	The maximum and minimum stored energies of EES
$SOC_{\max}^{TES}, SOC_{\min}^{TES}$	The maximum and minimum stored energies of TES
$SOC_{\max}^{HES}, SOC_{\min}^{HES}$	The maximum and minimum stored energies of HES

B. Binary Variables

U_t^{GT}	On/off status of GT at time t
$u_t^{EES}, u_t^{TES}, u_t^{HES}$	Charging/discharging statuses of EES, TES, and HES at time t

C. Continuous Variables

ΔE_t^r	Power adjustment quantity for equipment r at time t
C_{buy}	Energy purchase cost
C_{om}	Operation and maintenance cost
C_{cut}	Electricity curtailment cost
C_{adj}	Power adjustment cost
C_t^{EC}, C_t^{AC}	Output power of EC and AC at time t
E_t^r	Operating power of equipment r at time t, $E \in \{P, Q, H\}$
$G_t^{GT}, G_t^{GB}, P_t^{EL}$	Input power of GT, GB, and EL at time t
$H_t^{HFC}, P_t^{EC}, Q_t^{AC}$	Input power of HFC, EC, and AC at time t
$H_{C,t}^{HES}, H_{D,t}^{HES}$	Charging and discharging power of HES at time t
P_t^{GT}, Q_t^{GT}	Power generation and heat production of GT at time t
$P_{C,t}^{EES}, P_{D,t}^{EES}$	Charging and discharging power of EES at time t
P_t^{buy}, G_t^{buy}	Purchased electricity and gas power at time t
$Q_t^{GB}, H_t^{EL}, P_t^{HFC}$	Output power of GB, EL, and HFC at time t
$Q_{C,t}^{TES}, Q_{D,t}^{TES}$	Charging and discharging power of TES at time t
R_{CO2}	Carbon tax revenue
$SOC_t^{EES}, SOC_t^{TES}, SOC_t^{HES}$	Energy stored by EES, TES, and HES at time t

D. Random Variables

e_t^{WT}	Wind power forecasting error at time t
e_t^{PV}	Solar power forecasting error at time t
P_t^{WT}	Wind power at time t
P_t^{PV}	Solar power at time t

I. Introduction

INTEGRATED energy system (IES) has garnered significant attention in recent years as an efficient, reliable, and environmentally friendly energy utilization solution [1]. Through optimized scheduling and management, IES has the capability of integrating multiple forms of energy such as electricity, heat, hydrogen, and cooling to achieve efficient energy utilization and minimal environmental impact [2]. In addition, power-to-gas, carbon capture and storage [3], as well as shared energy storage technologies [4] also enable IES with the potential of low-carbon flexible operation under multi-energy flow. The hybrid energy storage system (HESS) combines various energy storage technologies such as batteries and thermal storage tanks, which effectively facilitates energy conversion, storage, and time-shifted energy transfer within the IES. This enhances the operational flexibility of the IES and promotes the integration of renewable energy sources [5], [6]. It is worth noting that in IES with HESS, the research of hydrogen energy storage (HES) and its related components such as electrolyzers (ELs) and hydrogen fuel cells (HFCs), has received extensive attention. By optimizing control and management, it can bring advantages to comprehensive utilization and safe operation of hydrogen energy [7], [8].

In recent years, many scholars have studied the application of HESS in IES. Reference [9] shows that expanding electric energy storage (EES) and thermal energy storage

(TES) could boost the economic benefit increase of IES by 8.23% and renewable energy consumption rate by 23.79%. Reference [10] introduces a multi-time-scale control strategy for IES using a combination of batteries, supercapacitors, and TES, enhancing power response, battery lifespan, and carbon emission reductions. Reference [11] develops an IES combining an organic Rankine cycle with hybrid energy storage, proving it is thermodynamically and economically feasible. Reference [12] simulates an IES for a coastal community in Hong Kong, China, showing that integrating EES, TES, and cooling energy storage could reduce carbon emissions by over 2600 tons and increase the renewable energy consumption rate to over 90%, while sensitivity analysis indicates that larger storage capacity does not always yield better results. Reference [13] offers a method for selecting energy storage types and capacities to improve IES economics and equipment lifespan. Reference [14] optimizes an electricity-hydrogen-thermal-gas IES with EES, TES, and HES, achieving cost reductions of 3.18% and carbon emission reductions of 5.05%. It is evident that considering hybrid energy storage technologies in the optimal scheduling of IES holds great promise.

However, the aforementioned studies rarely consider optimal scheduling methods across different time scales. The dynamic operating characteristics and response times of various energy devices within an IES are significantly different. Additionally, different energy storage systems exhibit distinct power response behaviors. As a result, the benefits of more refined control and scheduling of these storage devices across various time scales have not been fully explored in the optimal scheduling process.

Multi-time-scale scheduling optimization achieves optimization and adjustment through the division into two or three stages (such as day-ahead, intra-day, and real-time), and it is also an effective approach to address the volatility of wind and solar power within IES [15]. To this end, many scholars have conducted relevant research. Reference [16] takes into account the inertia of key inertial devices such as heat networks and combined heat and power units at multiple time scales, achieving coordinated dispatch of IES and improving its flexibility and precision. Reference [17] proposes a multi-objective optimal scheduling model for IES considering a multi-time-scale stepped carbon trading mechanism, which increases the economic benefits of IES by about 5% and the environmental benefits by about 2%. Reference [18] divides unit output into day-ahead and intra-day stages for planning and proposes a multi-time-scale optimal scheduling model for IES based on source-load forecasting, significantly improving the energy utilization rate of IES and flexibly reducing the impact of randomness on system operation. In [19], the demand response capability of the load is deeply explored, and a multi-time-scale scheduling strategy considering electrical and thermal loads is proposed based on the inertia effect of IES thermal loads. Unfortunately, although research on multi-time-scale optimal scheduling of IES has made progress, the intermittent and uncertain nature of wind and solar power with the continuous integration of high proportions of renewable energy poses significant challenges to the stable operation of IES [20]-[22]. In the aforementioned studies, the characterization of wind and solar uncertainties is primarily based on static forecasting errors, which may have serious consequences for the operation of IES in certain extreme scenarios.

In practical operations, robust optimization (RO), stochastic optimization (SO), and distributionally robust optimization (DRO) are the commonly used methods to address uncertainties such as those presented by renewable energy sources and load demands [23]. RO employs uncertainty sets to describe the fluctuation range of uncertain parameters, focusing on optimizing for the worst-case scenario, which often yields conservative optimal solutions [24]. RO is effective in handling the uncertainties of renewable energy and load demands by representing these factors through uncertainty sets, thereby enhancing the robustness of system operations while maintaining a relatively low computational complexity [25]-[29]. Unlike RO, SO typically assumes that random variables follow a specific probability distribution exactly and combats the interference of uncertainties in the system by generating a large number of random scenarios [30]. SO is regarded as an effective strategy to optimize operations in the face of uncertainties from wind and solar power generation, as well as load demands [31]-[33]. If the probability distribution of random variables within the system can be accurately determined, SO can improve the economic efficiency of system operations even in the presence of uncertainties [34]. The emerging DRO combines the features of both RO and SO, striking a balance between economic efficiency and robustness, and constructs ambiguity sets in a data-driven manner to represent random variables [35]. However, no matter based on moment [36] or probability distance [37], [38], the ambiguity sets present significant challenges in solving DRO models. Furthermore, existing research on addressing the uncertainties of renewable energy rarely considers the characteristic that forecasting errors decrease as the forecasting time scale is shortened, without distinguishing the optimal scheduling for dealing with renewable energy uncertainties under different time scales. In fact, by integrating the characteristics of multi-time-scale step-by-step optimal scheduling and employing different uncertainty optimization models to address wind and solar uncertainties at day-ahead, intra-day, and real-time stages, significant application prospects can be anticipated.

In summary, to address the shortcomings of existing studies, this paper proposes a multi-time-scale optimal scheduling method for the IES that considers the integration of EES, TES, and HES under wind and solar uncertainties. The method employs hybrid energy storage technologies and combines different optimization models to tackle renewable energy uncertainties under various time scales, aiming to enhance the overall economy and environmental friendliness of the system through optimal scheduling. Firstly, the proposed framework of IES with electric-thermal-hydrogen hybrid energy storage is established. Then, in response to the uncertainties of wind and solar power forecasting errors under long time scales (day-ahead) and short time scales (intra-day and real-time), RO scheduling model based on budget uncertainty set and SO scheduling model based on scenarios are proposed, respectively. Therefore, a multi-time-scale optimal scheduling method is put forward, which includes day-ahead RO, intra-day rolling SO, and real-time SO stages. Finally, the effectiveness of the proposed method is demonstrated through the case study, and the impacts of the uncertainty budget and hybrid energy storage on system benefits are analyzed.

II. Framework of IES

The framework of the IES discussed in this paper is depicted in Fig. 1. The primary energy flows within the IES encompass electric energy, thermal energy, hydrogen energy, cooling energy, and natural gas energy. The components that function in energy production and input roles include wind turbines (WTs), photovoltaic (PV) panels, the grid, and the natural gas network (NG). Intermediate energy conversion stages are populated by EL, HFC, gas turbines (GTs), gas boilers (GBs), electric chillers (ECs), and absorption chillers (ACs). The HESS consists of EES, TES, and HES. Finally, the energy consumption roles are fulfilled by four types of loads, i.e., electric, thermal, cooling, and hydrogen.

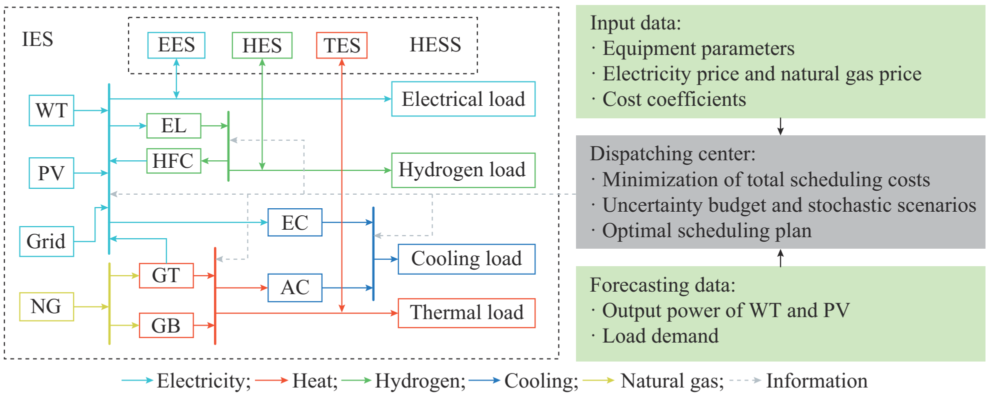

Fig. 1. Framework of IES.

The operation of the IES is centrally managed by the dispatching center. After receiving the forecasting data for WT, PV, and various loads, the dispatching center sends dispatching signals to the various devices and the HESS within the IES to minimize scheduling costs and obtain the optimal scheduling plan. Additionally, the dispatching center is responsible for handling uncertainties during the optimization process, which will be described in detail in subsequent sections.

III. Multi-time-scale Optimal Scheduling Method

Considering that the forecasting errors of renewable energy power decreases as the forecasting time scale is shortend, this paper proposes a multi-time-scale optimal scheduling method based on three stages, i.e., day-ahead, intra-day, and real-time. The multi-time-scale optimal scheduling process is illustrated in Fig. 2.

A. Day-ahead Robust Optimal Scheduling

1) Budget Uncertainty Set

In RO problems, the set space where uncertainty can occur is referred to as the uncertainty set. Using an appropriate representation of the uncertainty set is crucial for accurately assessing uncertainty. For classical RO problems, common representations of uncertainty sets include box, ellipsoidal, polyhedral, and budget sets. Each representation of the uncertainty set has its advantages and disadvantages, but the budget uncertainty set is constructed based on the relative values of uncertain parameter offsets, allowing for an accurate and straightforward description of the fluctuation of random variables [29].

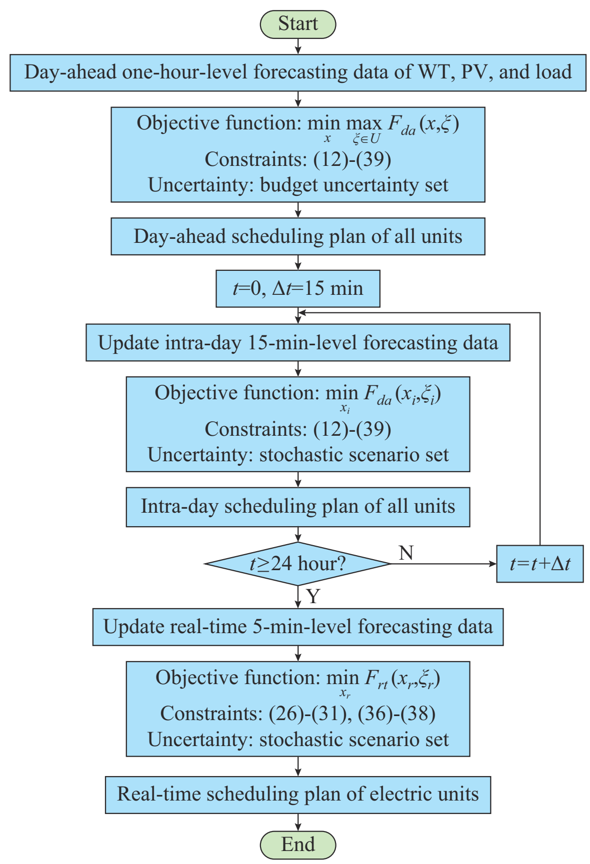

Fig. 2. Multi-time-scale optimal scheduling process.

Therefore, in this paper, we construct a budget uncertainty set to characterize the uncertainties of wind and solar power forecasting errors, with the constraint form represented as:

$$\underline{e}^{WT} \leq e_t^{WT} \leq \bar{e}^{WT} \tag{1}$$

$$\frac{\left| \hat{e}_t^{WT} - e_t^{WT} \right|}{\bar{e}^{WT} - \underline{e}^{WT}} \leq \Gamma_{WT} \tag{2}$$

$$\underline{e}^{PV} \leq e_t^{PV} \leq \bar{e}^{PV} \tag{3}$$

$$\frac{\left| \hat{e}_t^{PV} - e_t^{PV} \right|}{\bar{e}^{PV} - \underline{e}^{PV}} \leq \Gamma_{PV} \tag{4}$$

In this paper, we determine the boundaries of uncertain parameters by evaluating the intervals of historical data from the practical engineering. Subsequently, based on the budget uncertainty set, different ranges of uncertain parameters can be obtained through different values of Γ. Adjusting Γ allows for flexible control over the conservatism of the RO model solution.

Therefore, the power of wind and solar power can be expressed as:

$$P_t^{WT} = \hat{P}_t^{WT} + e_t^{WT} \tag{5}$$

$$P_t^{PV} = \hat{P}_t^{PV} + e_t^{PV} \tag{6}$$

2) Day-ahead Scheduling Model

The day-ahead scheduling aims to minimize the total scheduling cost F_{da} of the IES. The objective function comprises four parts: energy purchase cost C_{buy}, operation and maintenance cost C_{om}, electricity curtailment cost C_{cut}, and carbon tax revenue R_{CO2}. The expression for this objective function is given as:

$$F_{da} = C_{buy} + C_{om} + C_{cut} - R_{CO2} \tag{7}$$

$$C_{buy} = \sum_{t=1}^{T} \left(p_t^{grid} P_t^{buy} + p^{gas} G_t^{buy} \right) \tag{8}$$

$$C_{om} = \sum_{t=1}^{T} \sum_{r \in R} p_{om}^r E_t^r \tag{9}$$

$$C_{cut} = \sum_{t=1}^{T} \left(p_{cut}^{WT} P_{cut,t}^{WT} + p_{cut}^{PV} P_{cut,t}^{PV} \right) \tag{10}$$

$$R_{CO2} = \sum_{t}^{T} c_{CO2} \left[\delta_{re} \left(P_t^{WT} + P_t^{PV} \right) - \delta_q \left(G_t^{GT} + G_t^{GB} \right) - \delta_g P_t^{buy} \right] \tag{11}$$

In the scheduling process, each device needs to meet certain constraints during operation. The equipment operation constraints are given as:

$$P_t^{GT} = G_t^{GT} \eta_p^{GT} \tag{12}$$

$$P_{down}^{GT} \leq P_t^{GT} - P_{t-1}^{GT} \leq P_{up}^{GT} \tag{13}$$

$$U_t^{GT} P_{\min}^{GT} \leq P_t^{GT} \leq U_t^{GT} P_{\max}^{GT} \tag{14}$$

$$Q_t^{GT} = G_t^{GT} \eta_q^{GT} \tag{15}$$

$$Q_t^{GB} = G_t^{GB} \eta_q^{GB} \tag{16}$$

$$Q_{\min}^{GB} \leq Q_t^{GB} \leq Q_{\max}^{GB} \tag{17}$$

$$H_t^{EL} = P_t^{EL} \eta_h^{EL} \tag{18}$$

$$P_{\min}^{EL} \leq P_t^{EL} \leq P_{\max}^{EL} \tag{19}$$

$$P_t^{HFC} = H_t^{HFC} \eta_p^{HFC} \tag{20}$$

$$H_{\min}^{HFC} \leq H_t^{HFC} \leq H_{\max}^{HFC} \tag{21}$$

$$C_t^{EC} = P_t^{EC} \eta_c^{EC} \tag{22}$$

$$C_{\min}^{EC} \leq C_t^{EC} \leq C_{\max}^{EC} \tag{23}$$

$$C_t^{AC} = Q_t^{AC} \eta_c^{AC} \tag{24}$$

$$C_{\min}^{AC} \leq C_t^{AC} \leq C_{\max}^{AC} \tag{25}$$

Formulas (12)-(15) are the operation constraints of GT. GT converts natural gas into electricity and thermal energy through power generation and the recovery of heat from high-temperature gases. The ramp rate and on/off status of GT are constrained by (13) and (14), respectively. Equations (16)-(25) show the energy conversion relationships of GB, EL, HFC, EC, and AC and their power limits during operation.

The EES, TES, and HES all use state of charge (SOC) to indicate the energy they store. During operation, they must comply with energy constraints, power constraints, and the exclusivity constraints of charging/discharging. Additionally, within a scheduling period, they need to maintain a balance between charging and discharging. The operation constraints for these processes can be described as:

$$SOC_t^X = SOC_{t-1}^X + \left(E_{C,t}^X \eta_C^X - \frac{E_{D,t}^X}{\eta_D^X} \right) \Delta t \tag{26}$$

$$SOC_{\min}^X \leq SOC_t^X \leq SOC_{\max}^X \tag{27}$$

$$u_t^X E_{C,\min}^X \leq E_{C,t}^X \leq u_t^X E_{C,\max}^X \tag{28}$$

$$(1 - u_t^X) E_{D,\min}^X \leq E_{D,t}^X \leq (1 - u_t^X) E_{D,\max}^X \tag{29}$$

$$SOC_T^X = SOC_0^X \tag{30}$$

where the superscript X denotes the name of the storage device, including EES, TES, and HES; E is the power of different energy flows, including electricity (P), heat (Q), and hydrogen (H); Δt is the interval between scheduling periods; the subscript T denotes the end value of a scheduling cycle; and the subscript 0 denotes the initial value of a scheduling cycle.

In addition to the equipment operation constraints, the constraints of the day-ahead scheduling model also include energy balance constraints for electricity, heat, hydrogen, cooling, and natural gas, as well as constraints on wind and solar curtailment and energy purchase.

1) Energy balance constraints

$$\begin{aligned} & P_t^{buy} + P_t^{WT} + P_t^{PV} + P_t^{GT} + P_t^{HFC} + P_{D,t}^{EES} = \\ & \quad P_{cut,t}^{WT} + P_{cut,t}^{PV} + P_t^{EL} + P_t^{EC} + P_{C,t}^{EES} + P_t^{load} \end{aligned} \tag{31}$$

$$Q_t^{GT} + Q_t^{GB} + Q_{D,t}^{TES} = Q_t^{AC} + Q_{C,t}^{TES} + Q_t^{load} \tag{32}$$

$$H_t^{EL} + H_{D,t}^{HES} = H_t^{HFC} + H_{C,t}^{HES} + H_t^{load} \tag{33}$$

$$C_t^{EC} + C_t^{AC} = C_t^{load} \tag{34}$$

$$G_t^{buy} = G_t^{GB} + G_t^{GT} \tag{35}$$

2) Wind and solar curtailment constraints

$$0 \leq P_{cut,t}^{WT} \leq P_t^{WT} \tag{36}$$

$$0 \leq P_{cut,t}^{PV} \leq P_t^{PV} \tag{37}$$

3) Energy purchase constraints

$$0 \leq P_t^{buy} \leq P_{\max}^{buy} \tag{38}$$

$$0 \leq G_t^{buy} \leq G_{\max}^{buy} \tag{39}$$

In summary, the day-ahead RO scheduling model can be summarized as:

$$\begin{cases} \min\limits_{x} \max\limits_{\xi \in U} F_{da}(x, \xi) \\ \text{s. t. equipment operation constraints: (12)-(30)} \\ \quad \text{energy balance constraints: (31)-(35)} \\ \quad \text{wind and solar abandonment constraints: (36), (37)} \\ \quad \text{energy purchase constraints: (38), (39)} \end{cases} \tag{40}$$

where x represent the decision variables in the day-ahead scheduling model, including continuous variables indicating the operating power of various equipment and binary variables indicating the on/off status of the equipment; ξ represent the random variables denoting the wind and solar uncertainties, including e_t^{WT} and e_t^{PV}; U represents the uncertainty set of the RO model, as described by (1) to (4).

According to (40), the optimal solution can be obtained under the worst case of day-ahead WT and PV output, thus ensuring the robustness of day-ahead scheduling plan.

B. Intra-day Rolling SO Scheduling

1) Stochastic Scenario Set

The intra-day scheduling employs a scenario-based SO model. It generates a large number of initial scenarios for wind and solar power forecasting errors that satisfy specific probability distributions using Latin hypercube sampling (LHS). Subsequently, K-means clustering is applied to reduce the scenarios, resulting in a set of typical scenarios for wind and solar power forecasting errors, forming a stochastic scenario set. The detailed process refers to [39]. Then, the SO model determines the 15-min-level scheduling scheme through rolling scheduling. This paper assumes that the forecasting errors follow a normal distribution given as:

$$e_t^{WT} \sim N\left(\mu^{WT}, \sigma^{WT}\right) \tag{41}$$

$$e_t^{PV} \sim N\left(\mu^{PV}, \sigma^{PV}\right) \tag{42}$$

2) Intra-day Scheduling Model

The intra-day scheduling aims to minimize the total scheduling cost of the IES while minimizing power adjustments across various equipment as much as possible. The objective function incorporates the cost of equipment power adjustments C_{adj} in addition to the base of the prior scheduling.

$$F_{id} = C_{buy} + C_{om} + C_{adj} + C_{cut} - R_{CO2} \tag{43}$$

$$C_{adj} = \sum_{t=1}^{T} \sum_{r \in R} p_{adj}^{r} \Delta E_t^{r} \tag{44}$$

The constraints of the intra-day scheduling model include equipment operation constraints, energy balance constraints, wind and solar curtailment constraints, and energy purchase constraints. Additionally, the startup and shutdown states of GT should adhere to the day-ahead scheduling plan.

In summary, the intra-day scheduling model can be summarized as follows:

$$\begin{cases} \min\limits_{x_i} F_{id}(x_i, \xi_i) \\ \text{s.t. equipment operation constraints: (12)-(30)} \\ \quad \text{energy balance constraints: (31)-(35)} \\ \quad \text{wind and solar curtailment constraints: (36), (37)} \\ \quad \text{energy purchase constraints: (38), (39)} \end{cases} \tag{45}$$

where x_i represent the decision variables in the intra-day scheduling model, encompassing continuous variables denoting the operating power of each equipment and binary variables indicating the on/off status of the devices; and ξ_i represent the random variables for wind and solar uncertanties, including e_t^{WT} and e_t^{PV}, which conform to the stochastic scenarios determined by (41) and (42).

C. Real-time SO Scheduling

Considering the short-term fluctuations in electricity demand and wind and solar power, it is necessary to make real-time power adjustments to electric generation units. This involves swiftly responding with EES and adjusting measures such as purchasing or curtailing electricity to address any imbalances in power. At this stage, the same SO approach used in the intra-day stage is applied, so further elaboration is unnecessary here.

It is worth noting that the objective function and constraints of the real-time scheduling model only involve variables related to electric generation units. The real-time scheduling model can be summarized as:

$$\begin{cases} \min\limits_{x_r} F_{rt}(x_r, \xi_r) \\ \text{s. t. EES operation constraints: (26)-(30)} \\ \quad \text{electricity energy balance constraint: (31)} \\ \quad \text{wind and solar curtailment constraints: (36), (37)} \\ \quad \text{electricity purchase constraint: (38)} \end{cases} \tag{46}$$

where x_r represent the decision variables in the real-time scheduling model, including continuous variables such as the operating power of EES, wind and solar curtailment, and electricity purchase, as well as binary variables indicating the charging and discharging status of EES; and ξ_r represent the random variables for wind and solar uncertainties, including e_t^{WT} and e_t^{PV}, which comply with the stochastic scenarios determined by (41) and (42).

IV. CASE STUDY

A. Simulation Settings

The IES of a demonstration project in a coastal area of China on a typical day in summer is selected as a case study for this paper, as shown in Supplementary Material A Fig. SA1. The forecasting data for renewable energy output and various loads are illustrated in Supplementary Material A Fig. SA2, while the parameters of the system equipment are presented in Supplementary Material A Table SAI. It is assumed in this paper that the wind power forecasting error follows a normal distribution with an expectation of 0, an intra-day standard deviation of 3%, and a real-time standard deviation of 2%. Similarly, the solar power forecasting error is assumed to be with an expectation of 0, an intra-day standard deviation of 2%, and a real-time standard deviation of 1%. The modeling is conducted using the RSOME [40] toolbox in the MATLAB environment, using the Gurobi commercial solver for optimization.

B. Comparison of Various Scheduling Models

In order to compare and verify the advantages of the proposed model, the following scheduling models are set up in this section for simulation calculation.

1) Model 1: conduct day-ahead RO, and directly use it as the final scheduling plan. The forecasting errors are balanced by the grid, wind curtailment, and solar curtailment.

2) Model 2: conduct day-ahead RO, and then adjust power through intra-day rolling SO and real-time SO to obtain the final scheduling plan, which is the model proposed in this paper.

3) Model 3: conduct day-ahead SO, and then adjust power through intra-day rolling SO and real-time SO to obtain the final scheduling plan.

It is worth noting that in Model 3, the day-ahead SO assumes that the forecasting errors of WT and PV power follow a normal distribution, with a standard deviation of 5% for WT and 3% for PV. The simulation results are shown in Table I.

TABLE I
SCHEDULING COSTS IN VARIOUS MODELS

Model	Scheduling cost (¥10^3)					
	TSC	C_{buy}	C_{om}	C_{adj}	R_{CO2}	C_{cut}
1	1582.09	1409.98	206.55	0	53.95	19.51
2	1460.50	1284.89	207.54	12.16	61.26	17.17
3	1485.17	1297.54	207.13	25.83	63.11	17.78

By comparing Models 1 and 2, it can be observed that multi-time-scale scheduling can address day-ahead forecasting errors through intra-day and real-time power adjustments. Although Model 2 incurs additional power adjustment costs compared with Model 1, the overall cost of Model 2 is lower. This is because Model 1 can only rely on the grid and curtailment to balance day-ahead forecasting errors, whereas Model 2 can utilize local flexible resources such as GT for power adjustments. Additionally, due to the high carbon emission characteristics of the grid, the carbon tax revenue in Model 1 is also lower compared with that in Model 2.

By comparing Models 2 and 3, it is not difficult to find that in Model 3, the blind pursuit of economic efficiency at the day-ahead stage leads to increased intra-day and real-time adjustment costs. Additionally, the optimistic optimization approach in SO causes forecasting errors to be balanced by the grid and curtailment, resulting in higher energy purchase costs and curtailment costs compared with Model 2. This is detrimental to the operation of IES with a high proportion of renewable energy.

C. Analysis of Optimal Scheduling Results

1) Day-ahead Scheduling Analysis

In the day-ahead stage, to address the uncertainty caused by wind and solar power forecasting errors, an RO model based on budget uncertainty set is employed to obtain the scheduling scheme for the previous day. The day-ahead optimal scheduling results are depicted in Fig. 3, where “C” and “D” represent the charging and discharging of ESS, TES, or HES, respectively. From Fig. 3(a), it is evident that from 00:00 to 17:00, the supply of renewable energy generation is sufficient for the electric load. EL is activated during this period, converting a portion of the electric energy into hydrogen energy, while EES charges to absorb excess electricity. Furthermore, purchasing electricity from the grid happens during off-peak hours, maximizing the overall economic benefits of the scheduling. As indicated in Fig. 3(d), the primary source of cooling load comes from EC, mainly due to its high efficiency. AC only supplements a portion of the cooling load during peak periods (12: 00-23: 00). Combining Fig. 3(a) and (d) reveals that from 17:00 to 22:00, there is a peak in electricity and cooling demand. During this period, EES discharges the stored electricity from off-peak hours (00: 00-05: 00) to meet the demand. Figure 3(b) shows that due to its high heat efficiency, GB primarily handles the heat demand. GT is only utilized from 17:00 to 22:00 when electricity, heat, and cooling demands are all at high levels, maximizing the efficiency of combined heat and power generation. Additionally, TES stores excess heat during this period for later use. Combining Fig. 3(a) and (c) reveals that from 00: 00 to 05: 00, WT output exceeds the electricity demand. HES and EES utilize flexible conversion to absorb the surplus wind power. From 14: 00 to 19: 00, HES releases hydrogen to meet the hydrogen demand. In summary, the proposed optimal scheduling model effectively leverages the flexibility of IES and utilizes HESS to further enhance both economic and environmental benefits of the system.

2) Intra-day Scheduling Analysis

In the intra-day stage, based on the day-ahead plan, a rolling scheduling approach based on SO is employed, with the optimal scheduling results depicted in Fig. 4.

Due to inevitable discrepancies between short-term forecasting of wind, solar, and various loads and their prescheduled counterparts, adjustments to the power output of various devices are necessary throughout the intra-day rolling optimization process to ensure a balance between energy supply and demand.

Among these, EL and HFC, serving as flexible devices, exhibit considerable deviations in power output compared with the day-ahead results, aiming to fulfill the optimization objectives. Additionally, HESS involving EES, TES, and HES can be finely tuned at a 15-min time scale, thereby mitigating carbon emissions and reducing instances of curtailed power. The optimal scheduling results demonstrate the efficacy of the proposed method in adapting to the uncertainty of renewable energy power fluctuations and mitigating forecasting errors in short-term load forecasting.

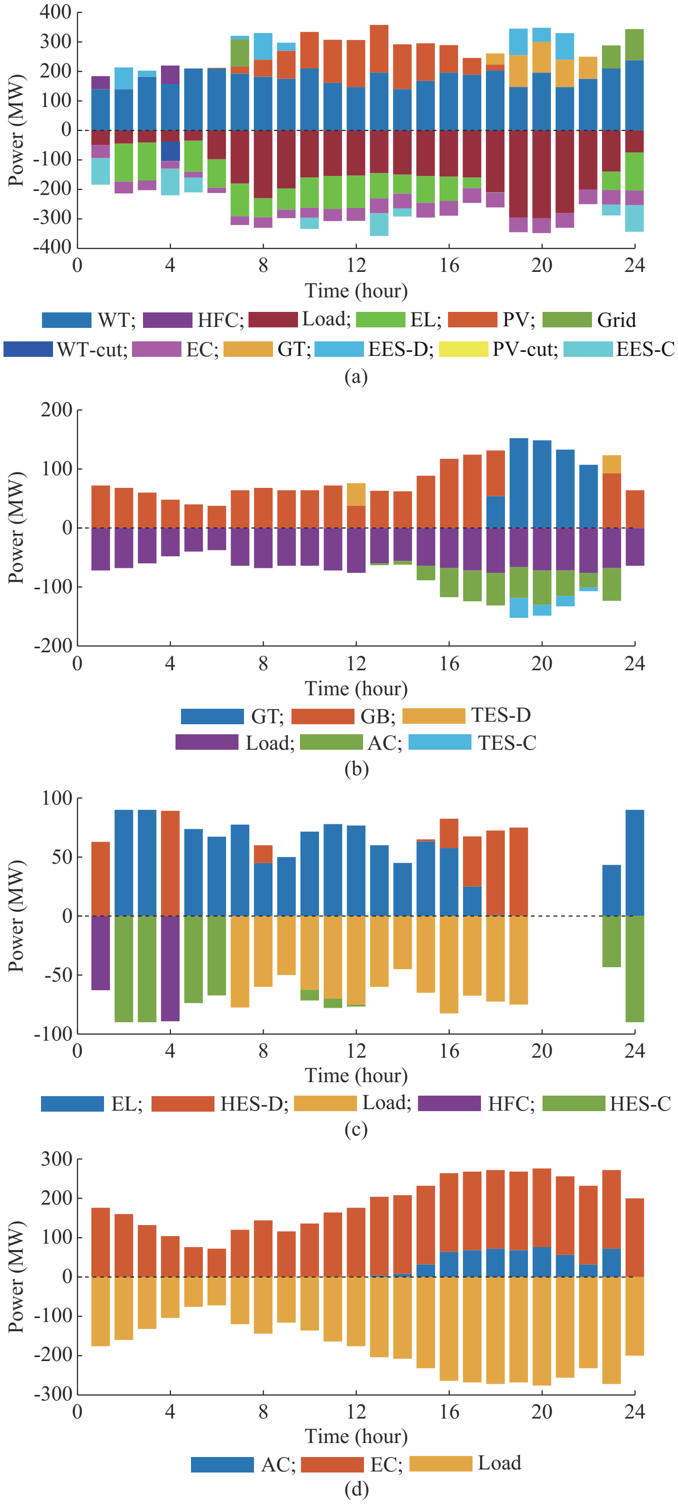

Fig. 3. Day-ahead optimal scheduling results. (a) Electric energy balance. (b) Thermal energy balance. (c) Hydrogen energy balance. (d) Cooling energy balance.

3) Real-time Scheduling Analysis

In the real-time stage, the issue of unbalanced electric power (UEP) primarily stems from short-term forecasting errors in wind, solar, and electric loads. These forecasting inaccuracies can lead to mismatches in power supply and demand, posing challenges to the stable operation of the IES.

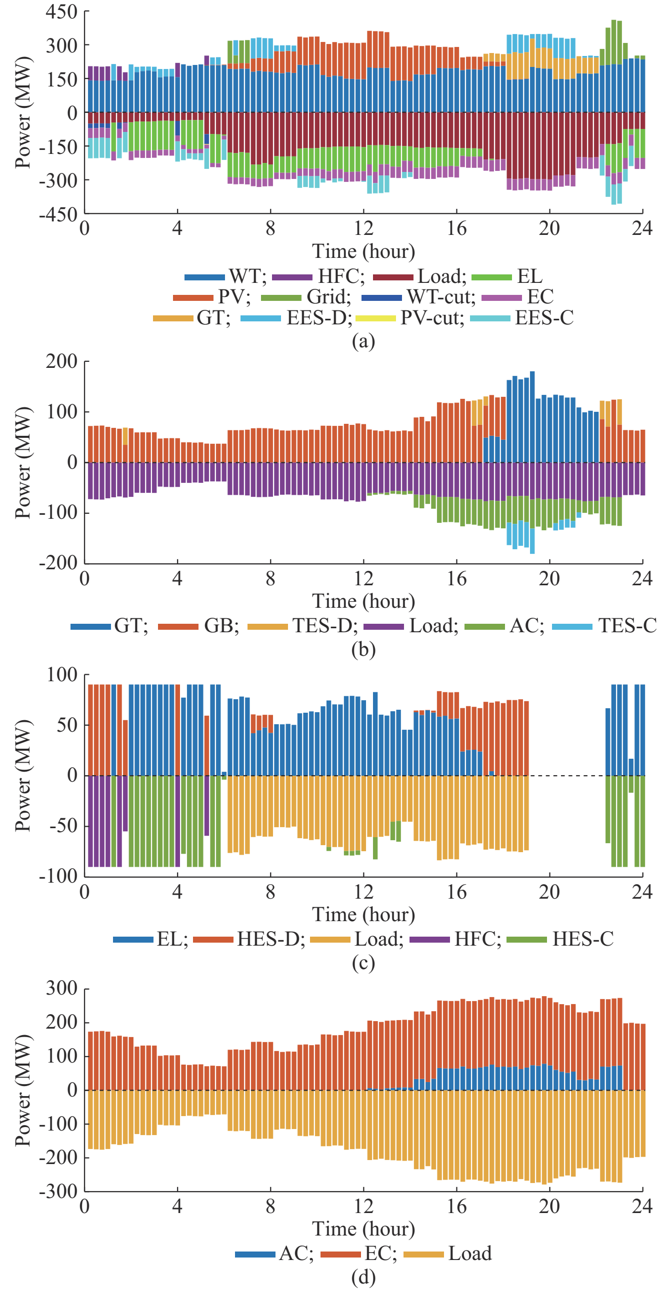

Fig. 4. Intra-day optimal scheduling results. (a) Electric energy balance. (b) Thermal energy balance. (c) Hydrogen energy balance. (d) Cooling energy balance.

In the real-time stage, the IES mitigates the UEP by adjusting the charging and discharging rates of EES, increasing or decreasing the amount of electricity purchased from the grid, and appropriately adjusting curtailed wind and solar power. The real-time power adjustment results are depicted in Fig. 5. As shown in Fig. 5, EES and the grid play a pivotal role in responding to fluctuations in wind, solar, and electric load power. Moreover, the rapid response of EES reduces the frequency of adjustments to purchased electricity, minimizing the impact on grid operation. Through the proposed method, the IES effectively meets the real-time scheduling requirements, further enhancing operational flexibility and facilitating energy supply-demand balance on a short-term scale.

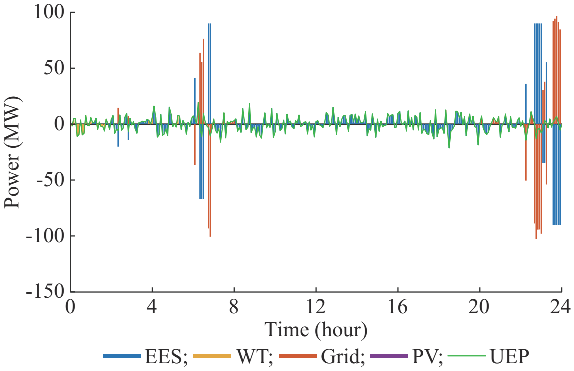

Fig. 5. Real-time power adjustment results.

Combining the optimal results across multiple time scales, Table II presents the scheduling costs for the three stages. It can be observed that from the day-ahead stage to the intra-day stage and then to the real-time stage, the total scheduling cost (TSC) gradually decreases. Compared with the day-ahead stage, TSC in the intra-day stage decreases by 5.5%, while in the real-time stage, it decreases by 3.12%. This demonstrates the advantages of the multi-time-scale optimal scheduling method proposed in this paper.

TABLE II
SCHEDULING COSTS OF DIFFERENT SCHEDULING STAGES

Stage	Scheduling cost (¥10^3)					
	TSC	C_{buy}	C_{om}	C_{adj}	R_{CO2}	C_{cut}
Day-ahead	1582.09	1409.98	206.55	0.00	53.95	19.51
Intra-day	1495.30	1320.95	207.52	11.83	61.55	16.55
Real-time	1448.67	1284.89	207.54	0.33	61.26	17.17

Additionally, the costs of purchasing electricity from the grid and gas from NG network constitute the largest portion of the total cost. In comparison to the day-ahead stage, the intra-day stage incurs additional operation costs and adjustment costs for equipment power. However, through flexible scheduling of HESS, the purchase cost significantly decreases, reducing the system reliance on the grid and NG. Meanwhile, carbon tax revenue increases by 14.09%, and electricity curtailment costs decrease by 15.17%.

D. Performance Analysis of Uncertainty Budget

In order to analyze the performance of the RO model in the day-ahead scheduling stage, the uncertainty budgets Γ_{WT} and Γ_{PV} in the budget uncertainty set for wind and solar forecasting errors were varied separately. The results of day-ahead TSC are shown in Fig. 6. From Fig. 6, it is evident that as the uncertainty budgets for wind and solar power forecasting errors increase within the budget uncertainty set, the TSC of the RO scheduling in the day-ahead period gradually rises. This is primarily because Γ_{WT} and Γ_{PV} reflect the range of fluctuations in wind and solar power forecasting errors. An expansion in this fluctuation range enhances the conservatism of the day-ahead RO scheduling, resulting in an increase in day-ahead TSC. Additionally, it is noticeable that the influence of Γ_{WT} and Γ_{PV} on TSC is more pronounced within the range of 0.2 to 0.5. When Γ_{WT} and Γ_{PV} exceed 0.5, the upward trend in TSC significantly diminishes because the random variables have approached their limits, and are constrained only by (1) and (3). Decision-makers can therefore choose the values of the uncertainty budgets flexibly, balancing between the optimism and risk in decision-making to attain the optimal scheduling solution.

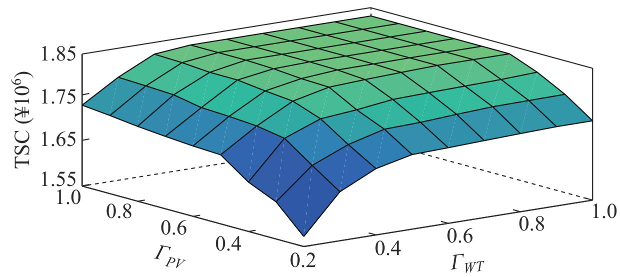

Fig. 6. Day-ahead TSC under different uncertainty budgets for wind and solar power forecasting errors.

E. Benefit Analysis of HESS

1) Comparison of Various Energy Storage Scenarios

To analyze the advantages of HESS, three different energy storage scenarios are set up in this part, as shown in Table III. Apart from the configuration of the energy storage devices, all other system parameters remain identical.

TABLE III
ENERGY STORAGE SCENARIO SETTING

Scenario	EES	TES	HES
1	√	×	×
2	√	√	×
3	√	√	√

The results of the intra-day optimization in the three energy storage scenarios are presented in Table IV. A comparison between Scenarios 1 and 2 reveals that the inclusion of TES reduces TSC but does not facilitate the integration of renewable energy sources, and may even exacerbate carbon emissions. This is because in the optimal scheduling with TES, there is a preference for activating GT for combined heat and power generation to provide more flexible resources, resulting in higher carbon emissions and compromising environmental benefits. Comparing Scenario 2 with Scenario 3 shows that with the addition of HES, both the overall economic and environmental benefits of the system are significantly improved. Through the flexible conversion of electric energy to hydrogen, surplus wind and solar power can be effectively utilized, reducing electricity curtailment while substantially increasing carbon tax revenue. Overall, although the inclusion of multiple energy storage devices may increase system operation costs and intra-day power adjustment costs, hybrid energy storage offers greater scheduling flexibility, reduces reliance on the grid and NG, and concurrently lowers carbon emissions, effectively adapting to the high penetration of renewable energy sources and meeting dual objectives of system economics and environmental sustainability.

TABLE IV
SCHEDULING COSTS IN THREE ENERGY STORAGE SCENARIOS

Scenario	Scheduling cost (¥10^3)					
	TSC	C_{buy}	C_{om}	C_{adj}	R_{CO2}	C_{cut}
1	1843.7	1519.50	185.21	3.40	−6.73	128.86
2	1837.3	1484.49	185.26	4.37	−34.32	128.86
3	1495.3	1320.95	207.52	11.83	61.55	16.55

2) Impact of HESS Capacity

The HESS capacity is a critical factor affecting the economic and environmental performance of the system. The carbon tax revenue, curtailment rate, and TSC under different capacity changes of energy storage device are obtained, as illustrated in Fig. 7. The EES and HES capacities significantly impact the carbon tax revenue, curtailment rate, and TSC. As the capacity increases, the TSC of the system decreases, carbon tax revenue increases, and the electricity curtailment phenomenon is notably improved. While an increase in TES capacity can enhance the economic efficiency of system dispatch, it does not contribute to environmental benefits.

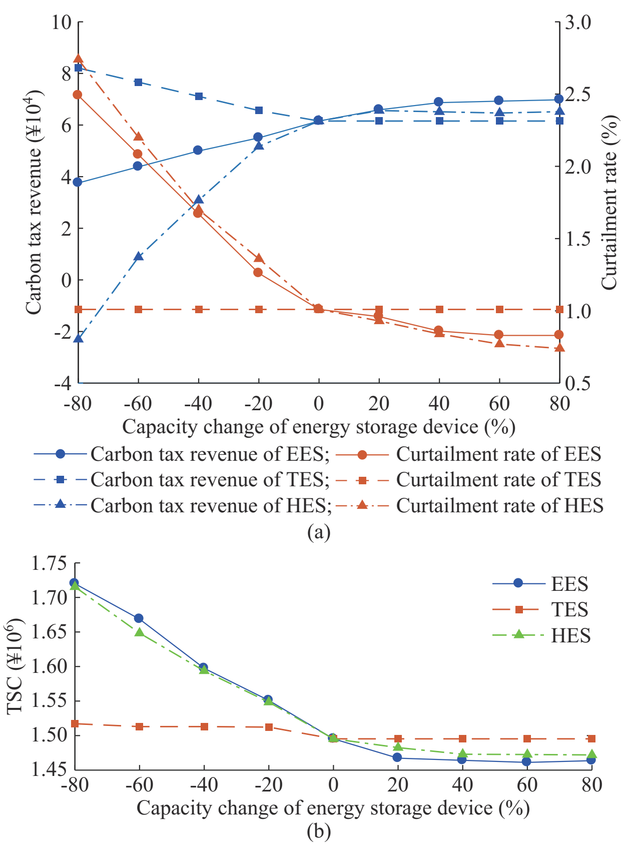

Fig. 7. Impact of energy storage capacity on scheduling cost. (a) Intra-day carbon tax revenue and curtailment rate. (b) Intra-day TSC.

Moreover, when the capacity reaches the designed level, the marginal benefits decrease significantly, further demonstrating the rationality of the capacity settings. Therefore, reasonably configuring the HESS capacity in IES can adapt to the wind and solar power uncertainties, reducing carbon emissions.

V. CONCLUSION

This paper establishes an IES model incorporating electric-thermal-hydrogen hybrid energy storage. It proposes a multi-time-scale optimal scheduling method comprising three stages: RO for day-ahead scheduling, rolling SO for intra-day scheduling, and real-time SO. Simulation results from the case study confirm the following conclusions.

1) With the multi-time-scale optimal scheduling method proposed in this paper, the total scheduling cost for the intra-day period decreases by 5.5% compared with the day-ahead period, and the total scheduling cost for real-time operations decreases by 3.12% compared with the intra-day period, demonstrating the effectiveness of the proposed method.

2) In the day-ahead stage, increasing the uncertainty budgets for wind and solar forecasting errors raises the total cost of robust optimal scheduling, with the most significant impact within the range of 0.2 to 0.5, beyond which the increase is slower, allowing decision-makers to balance economic efficiency and robustness.

3) The electric-thermal-hydrogen hybrid energy storage facilitates the flexible operation of IES and improves the economic and environmental benefits of IES. In addition to considering the marginal benefits, a reasonable design of HESS capacity is necessary.

Considering the flexibility resources on the user side of the IES, combined with integrated demand response, allowing hydrogen vehicles as hydrogen loads to respond to system scheduling, and exploring an optimized scheduling framework with multi-party collaboration will be the next research directions.

REFERENCES

[1] D. Song, W. Meng, M. Dong *et al.*, “A critical survey of integrated energy system: summaries, methodologies and analysis,” *Energy Conversion and Management*, vol. 266, p. 115863, Aug. 2022.
[2] Y. Luo, H. Hao, D. Yang *et al.*, “Multi-objective optimization of integrated energy systems considering ladder-type carbon emission trading and refined load demand response,” *Journal of Modern Power Systems and Clean Energy*, vol. 12, no. 3, pp. 828-839, May 2024.
[3] Y. Ma, H. Wang, F. Hong *et al.*, “Modeling and optimization of combined heat and power with power-to-gas and carbon capture system in integrated energy system,” *Energy*, vol. 236, p. 121392, Dec. 2021.
[4] Q. Li, X. Xiao, Y. Pu *et al.*, “Hierarchical optimal scheduling method for regional integrated energy systems considering electricity-hydrogen shared energy,” *Applied Energy*, vol. 349, p. 121670, Nov. 2023.
[5] F. Han, J. Zeng, J. Lin *et al.*, “Multi-stage distributionally robust optimization for hybrid energy storage in regional integrated energy system considering robustness and nonanticipativity,” *Energy*, vol. 277, p. 127729, Aug. 2023.
[6] M. Gao, Z. Han, C. Zhang *et al.*, “Optimal configuration for regional integrated energy systems with multi-element hybrid energy storage,” *Energy*, vol. 277, p. 127672, Aug. 2023.
[7] Q. Li, H. Wang, T. Wang *et al.*, “Online diagnosis method of water management faults based on hybrid-frequency electrochemical impedance spectroscopy for PEMFC,” *IEEE Transactions on Transportation Electrification*, vol. 11, no. 1, pp. 2707-2716, Feb. 2025.
[8] Q. Li, T. Su, L. Yin *et al.*, “Health management for PEMFC system long-term operation based on optimal temperature trajectory real-time optimization,” *IEEE Transactions on Industrial Electronics*, doi: 10.1109/TIE.2024.3436539

[9] Y. Wang, Y. Zhang, L. Xue *et al*., "Research on planning optimization of integrated energy system based on the differential features of hybrid energy storage system," *Journal of Energy Storage*, vol. 55, p. 105368, Nov. 2022.
[10] C. Pan, H. Fan, R. Zhang *et al*., "An improved multi-timescale coordinated control strategy for an integrated energy system with a hybrid energy storage system," *Applied Energy*, vol. 343 p. 121137, Aug. 2023.
[11] Y. Zhu, Y. Xu, H. Chen *et al*., "Optimal dispatch of a novel integrated energy system combined with multi-output organic Rankine cycle and hybrid energy storage," *Applied Energy*, vol. 343, p. 121113, Aug. 2023.
[12] M. Fan, S. Cao, and S. Lu, "Optimal allocation of multiple energy storage in the integrated energy system of a coastal nearly zero energy community considering energy storage priorities," *Journal of Energy Storage*, vol. 87, p. 111323, May 2024.
[13] M. Gao, Z. Han, B. Zhao *et al*., "Optimal planning method of multi-energy storage systems based on the power response analysis in the integrated energy system," *Journal of Energy Storage*, vol. 73, p. 109015, Dec. 2023.
[14] H. Dong, Z. Shan, J. Zhou *et al*., "Refined modeling and co-optimization of electric-hydrogen-thermal-gas integrated energy system with hybrid energy storage," *Applied Energy*, vol. 351, p. 121834, Dec. 2023.
[15] L. Wang, J. Lin, H. Dong *et al*., "Demand response comprehensive incentive mechanism-based multi-time scale optimization scheduling for park integrated energy system," *Energy*, vol. 270, p. 126893, May 2023.
[16] Y. Qin, P. Liu, and Z. Li, "Multi-timescale hierarchical scheduling of an integrated energy system considering system inertia," *Renewable and Sustainable Energy Reviews*, vol. 169, p. 112911, Nov. 2022.
[17] G. Zhu and Y. Gao, "Multi-objective optimal scheduling of an integrated energy system under the multi-time scale ladder-type carbon trading mechanism," *Journal of Cleaner Production*, vol. 417, p. 137922, Sept. 2023.
[18] X. Ma, B. Peng, X. Ma *et al*., "Multi-timescale optimization scheduling of regional integrated energy system based on source-load joint forecasting," *Energy*, vol. 283, p. 129186, Nov. 2023.
[19] J. Tang, J. Liu, T. Sun *et al*., "Multi-time-scale optimal scheduling of integrated energy system considering demand response," *IEEE Access*, vol. 11, pp. 135891-135904, Nov. 2023.
[20] S. Yao, W. Gu, S. Lu *et al*., "Dynamic optimal energy flow in the heat and electricity integrated energy system," *IEEE Transactions on Sustainable Energy*, vol. 12, no. 1, pp. 179-190, Jan. 2021.
[21] R. Ma, J. Song, Y. Zhang *et al*., "Lifetime-optimized energy management strategy for fuel cell unmanned aircraft vehicle hybrid power system," *IEEE Transactions on Industrial Electronics*, vol. 70, no. 9, pp. 9046-9056, Sept. 2023.
[22] H. Ming, B. Xia, K. Lee *et al*., "Prediction and assessment of demand response potential with coupon incentives in highly renewable power systems," *Protection and Control of Modern Power Systems*, vol. 5, no. 1, p. 12, Apr. 2020.
[23] R. Xie, W. Wei, M. Li *et al*., "Sizing capacities of renewable generation, transmission, and energy storage for low-carbon power systems: a distributionally robust optimization approach," *Energy*, vol. 263, p. 125653, Jan. 2023.
[24] Y. Xiang, J. Liu, and Y. Liu, "Robust energy management of microgrid with uncertain renewable generation and load," *IEEE Transactions on Smart Grid*, vol. 7, no. 2, pp. 1034-1043, Mar. 2016.
[25] J. Yang and C. Su, "Robust optimization of microgrid based on renewable distributed power generation and load demand uncertainty," *Energy*, vol. 223, p. 120043, May 2021.
[26] M. Aslani, M. Mashayekhi, H. Hashemi-Dezaki *et al*., "Robust optimal operation of energy hub incorporating integrated thermal and electrical demand response programs under various electric vehicle charging modes," *Applied Energy*, vol. 321, p. 119344, Sept. 2022.
[27] Z. Ma, Y. Zhou, Y. Zheng *et al*., "Distributed robust optimal dispatch of regional integrated energy systems based on admm algorithm with adaptive step size," *Journal of Modern Power Systems and Clean Energy*, vol. 12, no. 3, pp. 852-862, May 2024.
[28] Y. Lian, Y. Li, Y. Zhao *et al*., "Robust multi-objective optimization for islanded data center microgrid operations," *Applied Energy*, vol. 330, p. 120344, Jan. 2023.
[29] M. Tostado-Véliz, A. R. Jordehi, L. Fernandez-Lobato *et al*., "Robust energy management in isolated microgrids with hydrogen storage and demand response," *Applied Energy*, vol. 345, p. 121319, Sept. 2023.
[30] R. Li, S. Guo, Y. Yang *et al*., "Optimal sizing of wind/concentrated solar plant/electric heater hybrid renewable energy system based on two-stage stochastic programming," *Energy*, vol. 209, p. 118472, Oct. 2020.
[31] R. Yan, Z. Lu, J. Wang *et al*., "Stochastic multi-scenario optimization for a hybrid combined cooling, heating and power system considering multi-criteria," *Energy Conversion and Management*, vol. 233, p. 113911, Apr. 2021.
[32] C. Shao, C. Feng, M. Shahidehpour *et al*., "Optimal stochastic operation of integrated electric power and renewable energy with vehicle-based hydrogen energy system," *IEEE Transactions on Power Systems*, vol. 36, no. 5, pp. 4310-4321, Sept. 2021.
[33] A. Mobasseri, M. Tostado-Veliz, A. A. Ghadimi *et al*., "Multi-energy microgrid optimal operation with integrated power to gas technology considering uncertainties," *Journal of Cleaner Production*, vol. 333, p. 130174, Jan. 2022.
[34] X. Xu, W. Hu, W. Liu *et al*., "Optimal operational strategy for a future electricity and hydrogen supply system in a residential area," *International Journal of Hydrogen Energy*, vol. 47, no. 7, pp. 4426-4440, Jan. 2022.
[35] Q. Meng, X. Jin, F. Luo *et al*., "Distributionally robust scheduling for benefit allocation in regional integrated energy system with multiple stakeholders," *Journal of Modern Power Systems and Clean Energy*, vol. 12, no. 5, pp. 1631-1642, Sept. 2024.
[36] Y. Wang, M. Song, M. Jia *et al*., "Multi-objective distributionally robust optimization for hydrogen-involved total renewable energy CCHP planning under source-load uncertainties," *Applied Energy*, vol. 342, p. 121212, Jul. 2023.
[37] Y. Wang, Y. Yang, H. Fei *et al*., "Wasserstein and multivariate linear affine based distributionally robust optimization for CCHP-P2G scheduling considering multiple uncertainties," *Applied Energy*, vol. 306, p. 118034, Jan. 2022.
[38] Q. Wu and C. Li, "Modeling and operation optimization of hydrogen-based integrated energy system with refined power-to-gas and carbon-capture-storage technologies under carbon trading," *Energy*, vol. 270, p. 126832, May 2023.
[39] F. Mei, J. Zhang, J. Lu *et al*., "Stochastic optimal operation model for a distributed integrated energy system based on multiple-scenario simulations," *Energy*, vol. 219, p. 119629, Mar. 2021.
[40] Z. Chen, M. Sim, and P. Xiong, "Robust stochastic optimization made easy with RSOME," *Management Science*, vol. 66, no. 8, pp. 3329-3339, Aug. 2020.

Zhe Chen received the B.Sc. and Ph.D. degrees from the Department of Electrical Engineering, Zhejiang University, Hangzhou, China, in 2016 and 2021, respectively. He is currently an Engineer with State Grid Zhejiang Electric Power Research Institute, Hangzhou, China. His research interests include power system operation and planning, electric-hydrogen coupling system, and microgrid.

Zhihao Li received the B.S. and Ph.D. degrees in electrical engineering from the College of Electrical Engineering, Zhejiang University, Hangzhou, China, in 2012 and 2017, respectively. He is currently a Full-time Engineer in State Grid Zhejiang Electric Power Research Institute, Hangzhou, China. His research interests include power system optimization, renewable energy integration, and application of energy storage systems in power systems.

Da Lin received the B.Sc. and Ph.D. degrees from the Department of Electrical Engineering, Zhejiang University, Hangzhou, China, in 2011 and 2016, respectively. He is currently an Engineer with State Grid Zhejiang Electric Power Research Institute, Hangzhou, China. His research interests include smart grid and renewable energy integration.

Changjun Xie received the Ph.D. degree in vehicle engineering from Wuhan University of Technology (WHUT), Wuhan, China, in 2009. From 2012 to 2013, he was a Visiting Scholar at University of California Davis, Davis, USA. He is currently a Professor with the School of Automation, WHUT. His research interests include fuel cell system, control strategy of renewable vehicles, and thermoelectric power generation.

Zhewei Wang received the B.S degree in electrical engineering from the School of Automation, Wuhan University of Technology (WHUT), Wuhan, China, in 2022. He is currently pursuing the Ph.D. degree at the School of Automation, WHUT. His research interests include power system operation and planning, integrated energy system optimal scheduling, and microgrid.